Discover Geoscience

RESEARCH Open Access

Effects of Compton scattering on gamma-ray spectrometry applied to rocks from Irati Formation, Paraná sedimentary basin, Brazil

Eder Queiroz Barbosa[1], Daniel Marcos Bonotto[1*] and Gabrielle Roveratti Cecatto[1]

*Correspondence:
Daniel Marcos Bonotto
danielbonotto@yahoo.com.br
[1]IGCE-Instituto de Geociências e Ciências Exatas, UNESP-Universidade Estadual Paulista, Av. 24-A No. 1515, P.O. Box 178, Rio Claro, SP CEP 13506-900, Brasil

Abstract

Gamma-ray spectrometry is a useful technique that allows measuring the natural radiation emitted by K (^{40}K) and radionuclides belonging to the decay series of ^{238}U (eU = ^{226}Ra = ^{214}Bi) and ^{232}Th (eTh = ^{228}Th = ^{208}Tl) present in rock samples. Its evaluation is especially important for sedimentary rocks like those found at Irati Formation, Paraná Sedimentary Basin (PSB), Brazil, due to the possibility of finding stratigraphic marks associated with strong abrupt variations in the radioactivity levels during the surveys of sediment profiles. However, among the processes involved when gamma rays interact with matter, the Compton scattering is significant as it leaves its "signature" in gamma spectra recorded by different experimental arrangements, chiefly those utilizing scintillation detectors such as the NaI(Tl). This study describes the use of established stripping factor (RC) models and multiple linear regression (RLM) analysis to correct Compton interference in gamma-ray spectra to improve the calibration steps of a portable NaI(Tl) gamma spectrometer installed at LARIN-Ionizing Radiations Laboratory, UNESPETRO-IGCE-UNESP, Rio Claro (SP), Brazil. Afterwards, radiometric data in 111 rock samples from Irati Formation, São Paulo State, Brazil, were obtained, allowing determine gamma interference factors within the spectral windows of natural radionuclides [K(^{40}K), eU(^{214}Bi), and eTh(^{208}Tl)]. The statistical frequency distribution of the radioelement concentration data, considering the RLM approach, defined 11 classes whose range corresponded to 0–21.66% for K, 4.29–131.74 ppm for eU, and 12.01–388.46 ppm for eTh. Violin plots indicated that the data are normally distributed with one mode value and different shapes. For K, the highest difference was found for values obtained by a previous survey conducted in 2021, compared to those utilizing the methods RC and RLM. For eU and eTh data, the highest difference was verified for data obtained by the method RC relative to other approaches. The variation in the residues did not differ significantly for K among the three methods, whereas lesser variation was found between the RC and RLM methods for eU and eTh. Therefore, these findings allowed evaluating the influence of the Compton scattering on the monitoring realized, contributing to improving the accuracy and comprehension of gamma spectrometric data that are extensively used in geophysical surveys.

© The Author(s) 2025. **Open Access** This article is licensed under a Creative Commons Attribution-NonCommercial-NoDerivatives 4.0 International License, which permits any non-commercial use, sharing, distribution and reproduction in any medium or format, as long as you give appropriate credit to the original author(s) and the source, provide a link to the Creative Commons licence, and indicate if you modified the licensed material. You do not have permission under this licence to share adapted material derived from this article or parts of it. The images or other third party material in this article are included in the article's Creative Commons licence, unless indicated otherwise in a credit line to the material. If material is not included in the article's Creative Commons licence and your intended use is not permitted by statutory regulation or exceeds the permitted use, you will need to obtain permission directly from the copyright holder. To view a copy of this licence, visit http://creativecommons.org/licenses/by-nc-nd/4.0/.

Keywords Gamma ray analysis, NaI(Tl) detector, Compton scattering, Geophysical survey, Irati Formation, Paraná Sedimentary Basin

1 Introduction

Radioactivity plays a fundamental role in Geophysics by allowing geological mapping, mineral resource prospecting, and environmental radioactivity assessment, aiding in the interpretation of regional characteristics over large areas. The statistical nature of radioactive decay and the application of the Poisson distribution [55] are essential for understanding and modeling radioactive decay and other random events in various scientific fields, including Geophysics and related disciplines. Precise radiometric measurements require careful consideration of count statistics, background (BG) radiation, among other parameters.

Potassium (K), and the decay series of uranium (U) (^{238}U), actinium (^{235}U), and thorium (Th) (^{232}Th) have radionuclides that emit γ-rays with sufficient energy and intensity to be measured and have been widely monitored due to their abundance in the environment. The average crustal abundance for K is ~2–2.5%, for U is 2–3 ppm, and for Th is 8–12 ppm [16, 21, 25, 44, 45].

^{40}K (half-life = 1.3 Ga; abundance of 0.012% of natural K) decays to ^{40}Ca by β^--particle emission and to ^{40}Ar by electron capture, which is also accompanied by a gamma-ray emission [13]. ^{238}U (half-life = 4.46 Ga; abundance of 99.28% of natural U) is the parent nuclide in the (4n + 2) series, forming stable ^{206}Pb after 14 decays (8α and $6\beta^-$) [11, 35]. ^{232}Th (half-life = 13.9 Ga; abundance ~ 99.98% of natural Th) is the principal natural Th isotope, forming the (4n) decay series that finishes in the stable ^{208}Pb [29].

1.1 Gamma spectrometry with NaI(Tl) scintillation detectors

Since the 1960s, the mapping of the natural radioelements K, U and Th has been done with portable NaI(Tl) scintillation detectors for uranium exploration, geologic mapping and environmental studies [1–3, 19, 33, 37, 38, 42, 51]. Because neither ^{238}U nor ^{232}Th emits γ-rays, the gamma emissions from their radioactive daughter products are used to estimate their concentrations in the monitoring programs [29].

In gamma spectrometry, net counts represent the true number of gamma-rays detected from a specific radioactive source, after subtracting the BG radiation counts, whereas a photopeak is a local maximum in the gamma energy spectrum, representing the emission energy of photons of a radioactive source [28].

For gamma-spectrometers based on NaI(Tl) detectors, the readings have often been realized considering windows centered over the energy photopeaks of 1461 keV (^{40}K), 1765 keV (^{214}Bi), and 2615 keV (^{208}Tl), respectively, for the quantification of potassium, uranium, and thorium [27]. ^{214}Bi (half-life = 19.7 min) is a radionuclide generated within the ^{238}U decay series, whose measurements are generally reported as eU (equivalent uranium) in the literature [3, 21, 31, 53]. ^{208}Tl (half-life = 3.1 min) is a radionuclide generated within the ^{232}Th decay series, whose readings are commonly reported as eTh (equivalent thorium) in the literature [3, 31, 53].

Beyond cost, some major reasons for the successful applications of the NaI(Tl) detectors in a large number of gamma ray surveys include: easy to obtain in larger pieces doped with thallium; sensitivity to a wide energy range (0–3 MeV); applicability of

linearly converting the energy emitted by ionizing radiation into visible light; good scintillation efficiency; great robustness; reduced humidity sensitivity; and enhanced capacity to deal with higher counting rates without pulse pilling [33, 52].

1.2 Compton scattering highlights and objectives of this study

Reliable analysis through gamma ray spectrometry is a challenging task due to factors related to the gamma rays' interaction with matter, such as the photoelectric effect, Compton scattering, and pair production [33, 34]. The Compton scattering results in the creation of a recoil electron and a scattered gamma ray photon, while the Compton continuum corresponds to that part of the gamma energy spectrum formed by photons that have lost part of their original energies through Compton scattering [28]. Its effect in the gamma ray spectra is the generation of a Compton continuum of lower energy than that associated with the photopeak formed due to the photoelectric effect [41]. The Compton scattering causes peaks to overlap in the energy spectrum [4, 23, 30, 33, 54].

The gamma ray spectrum at low energies, where pair production is not significant, consists of a Compton continuum and a photopeak. As the incident photon energy decreases, the relative area of the photopeak increases. For energies below 100 keV, the Compton continuum may completely disappear. For intermediate energies, the possibility of multiple scattering followed by the escape of the last scattered photon allows the total deposited energy to be greater than the energy deposited by a single scattering event with escape of the scattered photon [33].

The Multichannel Analyzer (MCA) is a typical equipment utilized to record gamma ray spectra, in which are displayed windows (channels) of different γ-ray energies emitted by each radionuclide and a set of peaks related to nuclear transitions, each one corresponding to a specific radionuclide present in the sample [28]. The number of counts in each peak is proportional to the activity concentration of the radionuclide. One major challenge for such a purpose consists of getting reliable readings of the photopeaks present in the spectra, mainly removing interferences due to the Compton scattering process [3, 34]. This is because false anomalies associated with non-reliable data of net count rate may be pointed out, causing impacts on the interpretation of stratigraphic radiometric records for hydrocarbon exploration or lithological zoning, identification of mineral occurrences, and generation of ternary radiometric maps utilized for geological mapping, among other consequences [17, 18, 28, 40], etc.

This study focuses on the use of a portable gamma-spectrometer with a NaI(Tl) scintillation detector, presenting methods to optimize its analytical precision for readings of K, U, and Th. The main target of the investigation is to perform the Compton effect correction in gamma ray measurements as a contribution to improving the Geophysical understanding, but also with implications for radiological safety. Therefore, this paper addresses the importance of correcting the Compton scattering in the acquisition of gamma spectrometric data obtained by analyzing photopeaks above 300 keV, which can be affected by this effect. The careful selection of regions of interest (ROIs) in the photopeaks and the application of established stripping factor models and regression analysis to correct Compton interference for gamma spectrum analysis were utilized for data treatment of a selected site.

2 Experimental setup and calibration steps

The approach adopted here to correct the Compton interference on gamma ray spectra takes into account stripping factors, which allows for converting the counting rates obtained in the K, eU, and eTh windows into concentrations as described by Killeen and Carmichael [32], Kogan et al. [34], and Grasty and Darnley [22]. The definitions and notations correspond to those reported by Barbosa et al. [7], based on these authors, highlighting the stripping factors for correcting the Compton scattering in the gamma ray spectra as summarized in Table 1.

The matrix equations reported by Barbosa et al. [7] allow determining the K, U, and Th concentrations from the net count rates in the K, eU, and eTh windows. The multiple linear regression (RLM) analysis, as described by Killeen and Carmichael [32], also permits finding each interference factor contributing to the observed radioactivity, removing the effects chiefly caused by Compton scattering.

In this research, the experiments utilized a portable gamma-spectrometer with a planar EG&G ORTEC 2″ × 2″ NaI(Tl) scintillation crystal (digiDART model) installed at LARIN-Ionizing Radiations Laboratory, UNESPETRO-IGCE-UNESP, Rio Claro (SP), Brazil, which has an internal preamplifier and high-voltage power supply encapsulated within a robust aluminum housing (Fig. 1). It includes an adjustable high-voltage supply, an active polarization network, and a charge detection preamplifier. The incorporation of an active polarization network at the base of the photomultiplier tube (PMT) eliminates high-voltage cable connections with bulky external high-voltage sources. The active polarization network enables high operating rates with minimal peak variations. The 2BY2-DD model receives power through the digiDART-LF monitor. The weight of the whole equipment is approximately 4.6 kg.

The gamma-ray readings at LARIN were conducted under controlled temperature conditions (~20 °C), with possible spectral drifts over time monitored using a monoenergetic radioactive source of ^{137}Cs (activity = 0.1 μCi). The most prominent gamma-ray emitted during the ^{137}Cs decay is 661.7 keV, with approximately 85.1% of decays resulting in this energy, as the remaining decays involve lower energy gamma and X-rays [13].

For calibration of the gamma-spectrometer and to reduce the incidence of the BG radiation, lead shielding consisting of two rings of 20 cm-diameter, 4 cm-thick, and 8.5 cm-internal diameter was made and positioned as shown in Fig. 1, to avoid the contribution of incident lateral radiation on the detector. The analyses were realized using standards of KCl for readings of the ^{40}K window, pitchblende for readings of the ^{214}Bi window (eU), and monazite sand for readings of the ^{208}Tl window (eTh).

The pitchblende and monazite sand standards, having different certified uranium and thorium concentrations (NBL-102-A, NBL-104-A, NBL-105-A, NBL-107-A, NBL-109-A, and NBL-110-A), were provided by the New Brunswick Laboratory, U.S. Department of Energy, Argonne, Illinois, USA. Pure KCl (52 wt% in K, standard LII-KCl-1) and different mixtures prepared from this matrix and additions of pure SiO_2 were utilized to obtain variable potassium concentration. The following standards were prepared: LII-KCl-2 (54.16 g SiO_2 + 28.9 g KCl), LII-KCl-3 (80.12 g SiO_2 + 5.8 g KCl), LII-KCl-4 (82.11 g SiO_2 + 2.9 g KCl), and LII-KCl-5 (84.72 g SiO_2 + 0.5 g KCl). Table 2 describes the relevant data of the standards utilized. The BG readings were done using a 99.9% purity silica matrix [7], adopting the same geometry of the standards.

Table 1 Relevant parameters for analyzing gamma ray spectra taking into account stripping factors for the Compton scattering removal (RC)

Parameter	Meaning	Definition	Remark
nK_{gross}	Gross counting rate in K window	Total number of counts in K peak divided by the counting time	
nU_{gross}	Gross counting rate in eU window	Total number of counts in ^{214}Bi peak divided by the counting time	
nTh_{gross}	Gross counting rate in eTh window	Total number of counts in ^{208}Tl peak divided by the counting time	
$nKBG$	BG counting rate in K window	Number of BG counts in K window divided by the counting time	
$nUBG$	BG counting rate in eU window	Number of BG counts in ^{214}Bi window divided by the counting time	
$nThBG$	BG counting rate in eTh window	Number of BG counts in ^{208}Tl window divided by the counting time	
$(nK)_{net}$	K net counting rate	$nK_{gross} - nKBG$	Strobino [50]
$(nU)_{net}$	eU net counting rate	$nU_{gross} - nUBG$	Strobino [50]
$(nTh)_{net}$	eTh net counting rate	$nTh_{gross} - nThBG$	Strobino [50]
$a = a_{U,Th}/a_{Th,Th}$	Correction factor due to the interference of the eU peak on the eTh window	Stripping factor for correcting the Compton scattering	Killeen and Carmichael [32]
$\beta = a_{K,Th}/a_{Th,Th}$	Correction factor due to interference of the K peak on the eTh window	Stripping factor for correcting the Compton scattering	Killeen and Carmichael [32]
$\gamma = a_{K,U}/a_{U,U}$	Correction factor due to interference of the K peak on the eU window	Stripping factor for correcting the Compton scattering	Killeen and Carmichael [32]
$a = a_{Th,U}/a_{U,U}$	Correction factor due to interference of the eTh peak on the eU window	Stripping factor for correcting the Compton scattering	Killeen and Carmichael [32]
$b = a_{Th,K}/a_{K,K}$	Correction factor due to interference of the eTh peak on the K window	Stripping factor for correcting the Compton scattering	Killeen and Carmichael [32]
$g = a_{U,K}/a_{K,K}$	Correction factor due to interference of the eU peak on the K window	Stripping factor for correcting the Compton scattering	Killeen and Carmichael [32]
$(nK)_{net'}$	K net counting rate	$(nK_{gross}) - \gamma\,(nU)_{net} - \beta\,(nTh)_{net}$	Considering the stripping factors for correcting the Compton scattering
$(nU)_{net'}$	eU net counting rate	$(nU_{gross}) - a\,(nTh)_{net} - g\,(nK)_{net}$	Considering the stripping factors for correcting the Compton scattering
$(nTh)_{net'}$	eTh net counting rate	$(nTh_{gross}) - a\,(nU)_{net} - b\,(nK)_{net}$	Considering the stripping factors for correcting the Compton scattering
C_K	K concentration	$C_K = (nK)_{net'}/S_K$	$S_K = a_{K,K}$, sensitivity constant for K
C_U	eU concentration	$C_U = (nU)_{net'}/S_U$	$S_U = a_{U,U}$, sensitivity constant for U
C_{Th}	eTh concentration	$C_{Th} = (nTh)_{net'}/S_{Th}$	$S_{Th} = a_{Th,Th}$, sensitivity constant for Th

The data obtained for the silica readings allowed for the determination of the Critical Level and Detection Limit [15] for the gamma ray measurements by the spectrometric system (Table 3). These values are important for validating the data obtained by removing the BG, which, due to variability and the detector's spectral drift, may present

Fig. 1 2BY2-DD (2″ × 2″) NaI(Tl) scintillation detector from EG&G ORTEC, digiDART-LF monitor, and lead shielding rings utilized during the gamma-ray readings

Table 2 Standards utilized for calibration of the portable gamma-spectrometer and corresponding windows (channels) for readings of ^{40}K (K), ^{214}Bi (eU), and ^{208}Tl (eTh)

			Channels			Concentration		
Standard	**Weight (g)**	**Time (s)**	**K**	**U**	**Th**	**K (%)**	**eU (ppm)**	**eTh (ppm)**
LII-KCL-1	50.00	2001.92	754–886	940–1054	1380–1528	52	0	0
LII-KCL-2	50.00	3924.10	754–886	940–1054	1380–1528	25	0	0
LII-KCL-4	50.00	10,336.22	754–886	940–1054	1380–1528	2.5	0	0
LII-KCL-5	50.00	19,984.18	754–886	940–1054	1380–1528	0.5	0	0
NBL-102-A	50.00	956.68	754–886	940–1054	1380–1528	0	1025.0	0
NBL-104-A	48.06	3597.54	754–886	940–1054	1380–528	0	98.8	0
NBL-105-A	50.00	10,583.88	754–886	940–1054	1380–1528	0	10.2	0
NBL-107-A	50.00	1111.88	754–886	940–1054	1380–1528	0	40.0	1,028.0
NBL-109-A	48.96	2482.40	754–886	940–1054	1380–1528	0	4.0	105.2
NBL-110-A	50.00	6658.38	754–886	940–1054	1380–1528	0	0.4	10.4
BG SiO_2	28.00	20,000.00	754–886	940–1054	1380–1528	0	0	0

negative net values for samples with low concentrations of the studied natural radioelements, and also due to the unavailability of standards with intermediate concentrations of isolated radionuclides (less than 20% for ^{40}K and 50 ppm for eU and eTh) and some standards that provide the same intermediate concentrations for all 3 radioelements. This is the case for standards NBL107-A, NBL-109-A, and NBL-110A, whose composition combines monazite (^{232}Th) and pitchblende (^{238}U).

Table 3 Critical level (LC) and detection limit (LD) of the gamma spectrometer as determined from readings of the high purity silica sample

K	U	Th
Gross area (GA, counts)		
17,361 ± 131.76	5089 ± 71.34	2681 ± 51.78
Counting rate (Tc, cpm)		
52.08 ± 0.40	15.27 ± 0.21	8.04 ± 0.16
LC (cpm)		
0.92 ± 3.04E−04	0.50 ± 4.14E−04	0.36 ± 4.86E−04
LC (cpm/g)		
0.03 ± 1.09E−05	0.02 ± 1.48E−05	0.01 ± 1.73E−05
LD (cpm)		
1.83 ± 6.02E−04	0.99 ± 8.19E−04	0.72 ± 9.61E−04
LD (cpm/g)		
0.07 ± 2.15E−05	0.04 ± 2.92E−05	0.03 ± 3.43E−05

Table 4 presents the obtained and calculated data for applying the methods for the removal of the Compton interference. The data presented are from the gamma spectrometric analysis of the standards done by Cecatto [10], whose spectra were quantified for the 3 intervals of interest by establishing 3 fixed windows (channels) to minimize significant variations from spectral drift, especially due to variations in background radiation and interference, which can increase the errors propagation in the number of counts.

The graphs and mathematical equations detailing, step by step, the calculations realized to evaluate the interferences in the spectral windows of interest, according to the concentrations of the 3 natural radioelements of interest are given in the Supplementary Material, from which it was possible to define the concentration equations for K(%), eU (ppm), and eTh (ppm) as shown in Fig. 2, expressing the data interpolation after removing the Compton interference in the effective intensity readings of the standards.

The procedure for the system calibration consists of the use of the "Multiple Linear Regression" (RLM), which utilizes the "Least Squares" method as a tool capable of predicting the correlation between different variables and how they can influence the quantitative determination of each other. For its application, the fundamental principle is based on net count values in the gamma spectrum of the standards and, subsequently, of the samples to be analyzed using this model.

Thus, the RLM allowed obtaining the corresponding coefficients for calculating the concentrations related to the counts (Table 5), in the 3 intervals of interest, yielding the C_K, $C_{U,}$ and C_{Th} concentrations as also shown in Table 5, whose residual errors in the adjusted equations correspond to about 9, 4 and 12.5%, respectively.

3 Study area

The equations shown in Fig. 2 were used to calculate the interferences of Compton scattering in the gamma spectra obtained by Cecatto [10] for all rock samples analyzed, which were from the Irati Formation, thus allowing for a comparison of the differences found in the data treatment. This formation exposes the entire Permian section of the Paraná Sedimentary Basin (PSB), including the Itararé Group, of Permo-Carboniferous age, the Tatuí Formation (Guatá Group), and the Passa Dois Group (Irati and Corumbataí formations). The Irati Formation is subdivided into two members: Taquaral and Assistência [6, 26, 39].

Table 4 Parameters obtained in the readings of ^{40}K (K), ^{214}Bi (eU), and ^{208}Tl (eTh) for the standards utilized for calibration of the gamma-spectrometer

Parameter	Unit	LII-KCL-1	LII-KCL-2	LII-KCL-4	LII-KCL-5	NBL-102-A	NBL-104-A	NBL-105-A	NBL-107-A	NBL-109-A	NBL-110-A
Gross area (GA)											
nK	Counts	4348.00 ± 65.94	5709.00 ± 75.56	9591.00 ± 97.93	17,039.00 ± 130.53	3303.00 ± 57.47	3903.00 ± 62.47	10,534.00 ± 102.64	1655.00 ± 40.68	2292.00 ± 47.87	5680.00 ± 75.37
nU	Counts	536.00 ± 23.15	1054.00 ± 32.47	2736.00 ± 52.31	4846.00 ± 69.61	1861.00 ± 43.14	1421.00 ± 37.70	2987.00 ± 54.65	717.00 ± 26.78	734.00 ± 27.09	1566.00 ± 39.57
nTh	Counts	264.00 ± 16.25	518.00 ± 22.76	1504.00 ± 38.78	2586.00 ± 50.85	156.00 ± 12.49	479.00 ± 21.89	1595.00 ± 39.94	667.00 ± 25.83	471.00 ± 21.70	892.00 ± 29.87
Counting rate											
rK	cpm	130.31 ± 1.98	87.29 ± 1.16	55.67 ± 0.57	51.16 ± 0.39	207.15 ± 3.60	65.09 ± 1.04	59.72 ± 0.58	89.31 ± 2.20	55.40 ± 1.16	51.18 ± 0.68
rU	cpm	16.06 ± 0.69	16.12 ± 0.50	15.88 ± 0.30	14.55 ± 0.21	116.72 ± 2.71	23.70 ± 0.63	16.93 ± 0.31	38.69 ± 1.44	17.74 ± 0.65	14.11 ± 0.36
rTh	cpm	7.91 ± 0.49	7.92 ± 0.35	8.73 ± 0.23	7.76 ± 0.15	9.78 ± 0.78	7.99 ± 0.37	9.04 ± 0.23	35.99 ± 1.39	11.38 ± 0.52	8.04 ± 0.27
Tc–BG SiO_2											
Net K	cpm	78.23 ± 2.02	35.21 ± 1.22	3.59 ± 0.69	−0.93 ± 0.56	155.07 ± 3.63	13.01 ± 1.11	7.63 ± 0.70	37.23 ± 2.23	3.32 ± 1.22	−0.90 ± 0.79
Net U	cpm	0.80 ± 0.73	0.85 ± 0.54	0.62 ± 0.37	−0.72 ± 0.30	101.45 ± 2.71	8.43 ± 0.66	1.67 ± 0.38	23.42 ± 1.46	2.47 ± 0.69	−1.16 ± 0.42
Net Th	cpm	−0.13 ± 0.51	−0.12 ± 0.38	0.69 ± 0.27	−0.28 ± 0.22	1.74 ± 0.80	−0.05 ± 0.40	1.00 ± 0.27	27.95 ± 1.40	3.34 ± 0.55	−0.01 ± 0.31
Validated data											
K	cpm	78.23 ± 2.02	35.21 ± 1.22	3.59 ± 0.69	0.92 ± 0.56	155.07 ± 3.63	13.01 ± 1.11	7.63 ± 0.70	37.23 ± 2.23	3.32 ± 1.22	0.92 ± 0.79
U	cpm	0.80 ± 0.73	0.85 ± 0.54	0.62 ± 0.37	0.50 ± 0.30	101.45 ± 2.71	8.43 ± 0.66	1.67 ± 0.38	23.42 ± 1.46	2.47 ± 0.69	0.50 ± 0.42
Th	cpm	0.36 ± 0.51	0.36 ± 0.38	0.69 ± 0.27	0.36 ± 0.22	1.74 ± 0.80	0.36 ± 0.40	1.00 ± 0.27	27.95 ± 1.40	3.34 ± 0.55	0.36 ± 0.31
Effective intensity											
IK	cpm/g	1.56 ± 0.04	0.70 ± 0.02	0.07 ± 0.01	0.02 ± 0.01	3.10 ± 0.07	0.27 ± 0.02	0.15 ± 0.01	0.74 ± 0.04	0.07 ± 0.02	0.02 ± 0.02
IU	cpm/g	0.02 ± 0.01	0.02 ± 0.01	0.01 ± 0.01	0.01 ± 0.01	2.03 ± 0.05	0.17 ± 0.01	0.03 ± 0.01	0.47 ± 0.03	0.05 ± 0.01	0.01 ± 0.01
ITh	cpm/g	0.01 ± 0.01	0.01 ± 0.01	0.01 ± 0.01	0.01 ± 0.00	0.03 ± 0.02	0.01 ± 0.01	0.02 ± 0.01	0.56 ± 0.03	0.07 ± 0.01	0.01 ± 0.01

The Irati Formation corresponds to the basal unit of the Passa Dois Group in the PSB. Despite its small thickness, it exhibits unique lithofacial characteristics, including evaporites and the alternation of dolomitic limestones and bituminous shales [36]. Current interest in the Irati Formation has increased due to the growing quest to understand the occurrences of oil in limestone fractures. This formation contains bituminous shales from the Permian period, which have potential for generating liquid hydrocarbons.

The lithology of the Irati Formation varies considerably in terms of the proportions of limestone and shale, but its characteristics are similar and distinct, making it an excellent and fundamental formation for the stratigraphic study of Gondwana. It is common to observe an alternation of two sets of layers with differences in thickness in occurrences of the formation located further north, such as in areas near Limeira city and Assistência District (Rio Claro city), in which the sample collection was done [10]. The sampling of 111 rock specimens was conducted along one wall in three distinct sections (upper, middle, and lower), corresponding to different types of lithotypes (limestone, shale, and diabase) as detailed by Cecatto [10] and Roveratti and Bonotto [46], and also shown in the Supplementary Material. The diabases are from the Cretaceous, comprising intrusive igneous bodies within the Irati Formation. The diabase occurrence motivated the development of several studies aimed at understanding the effects of magmatism on carbonatic rocks, to solve technical problems related to oil and gas exploration [49].

In general, shales exhibit higher levels of natural radioactivity due to K, U, and Th compared to carbonates, primarily because of their presence in clay minerals and organic matter within the silicic matrix [21, 29]. However, some carbonates may sometimes have higher radioactivity if they contain shaly horizons, uranium mineralization, or are rich in organic matter [18, 21]. Thus, the Compton correction is relevant for interpreting these lithologies of the Irati Formation, as it can help to discriminate similar gamma-ray responses between shales and limestones due to scattering effects.

All rock samples for analysis were crushed to a grain size of 0.177–0.053 mm and inserted into 62-mm diameter and 23-mm high cylindrical containers made of both metallic and plastic materials, similar to those described by the IAEA [28]. It is important to emphasize that the adopted geometry and related efficiency of the gamma detection were the same for the standards and each rock sample analyzed. Figure 3 illustrates a flow chart summarizing the main steps involved in the gamma-ray analysis of the rock samples.

4 Results and discussion

The most relevant data for calculating the interference of Compton scattering in the gamma spectra obtained by Cecatto [10] are reported in the Supplementary Material. Figure 4 shows a comparison of the gross counting rate/weight for K, U, and Th as measured by Cecatto [10] with the net counting rate/weight calculated in this paper for all rock samples from the Irati Formation. The gross values are higher than the net ones, as expected.

Figure 5 shows the results obtained when the equations shown in Fig. 2 are applied for the removal of the interferences of Compton scattering in the gamma spectra of all rock samples from the Irati Formation. As a consequence of the gamma readings of the standards, very incipient and practically constant Compton scattering interference was found in the thorium photopeak due to potassium and uranium occurring in the rocks.

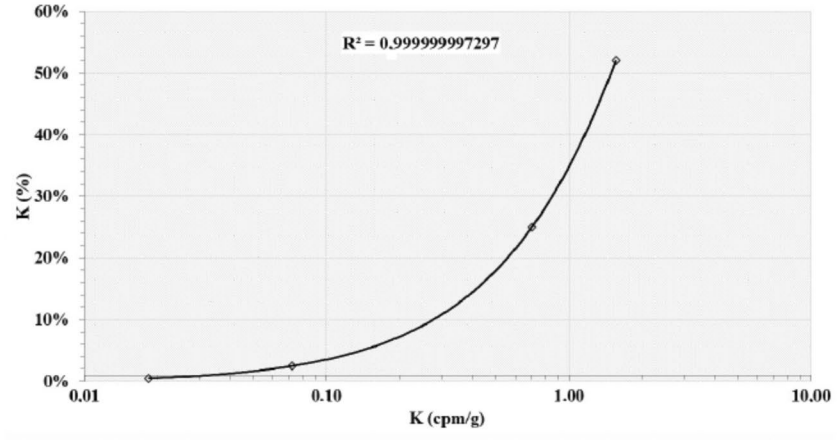

$$C_K = -0.028138167916.I_K{}^2 + 0.377624698003.I_K - 0.001960704702$$

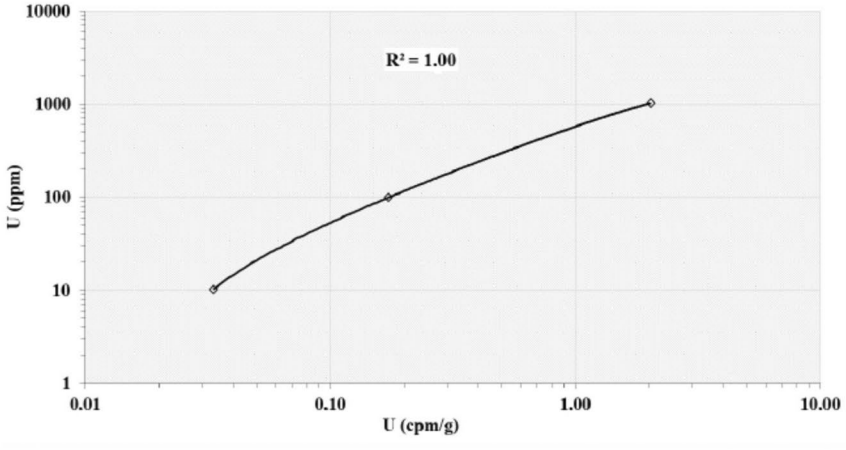

$$C_U = -69.655273627897.I_U{}^2 + 652.154929988065.I_U - 11.456335894925$$

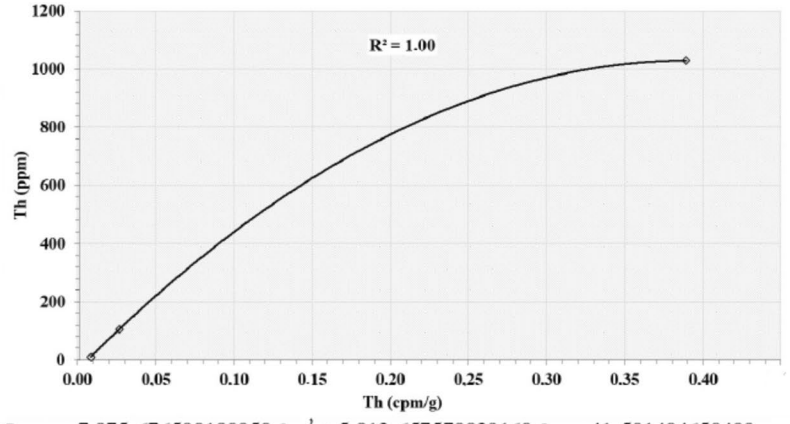

$$C_{Th} = -7{,}875.676590180950.I_{Th}{}^2 + 5{,}813.657578829160.I_{Th} - 41.501404650499$$

Fig. 2 Interpolation of the data for defining a mathematical model for calculating (*top*) C_K, (*middle*) C_U, and (*bottom*) C_{Th} after removing Compton interference in the emission intensity of the standards

Table 5 Coefficients and equations obtained by RLM for calculating concentrations through the effective intensity (cpm/g) of K, U, and Th

Coefficients	C_K	C_U	C_{Th}
Intersection	−0.001391953 ± 0.007113079	1.401364942 ± 2.466627287	−17.15404203 ± 3.934625575
I_K[a]	0.342763417 ± 0.011383659	−5.639789493 ± 0.3947551287	–
IU[a]	−0.523059897 ± 0.017927527	519.7437819 ± 6.216791367	−23.67222872 ± 5.666653962
I_{Th}[a]	−0.015709307 ± 0.0032775901	−358.935172 ± 11.36581421	1887.439063 ± 20.79248429
Equations			
$C_K(\%) = 0.3428 \times I_K - 0.5231 \times I_U - 0.0157 \times I_{Th} - 0.0014$			
$C_U(ppm) = -5.6398 \times I_K + 519.7438 \times I_U - 358.9352 \times I_{Th} + 1.4014$			
$C_{Th}(ppm) = -23.6722 \times I_U + 1887.4391 \times I_{Th} - 17.1540$			

[a] I_K, I_U, and I_{Th} correspond to the effective intensity (count rate per mass, cpm/g) in the photopeaks associated with K, U, and Th, respectively

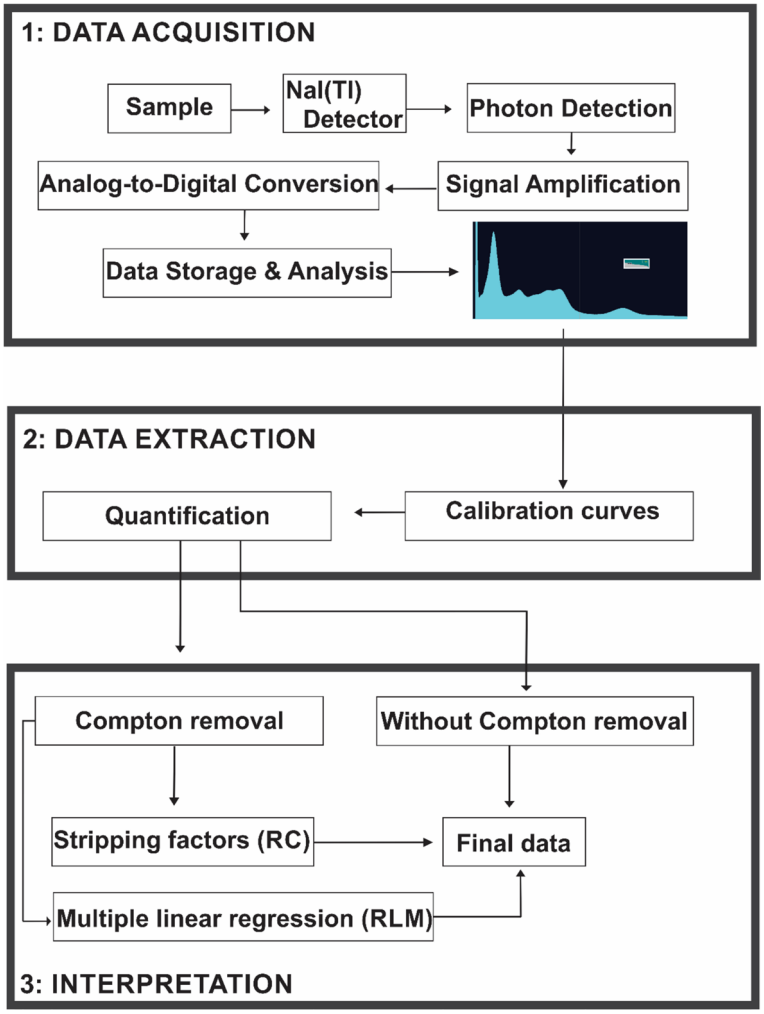

Fig. 3 A flow chart showing the methodology for the data acquisition of gamma-ray spectrometry with NaI(Tl) scintillation detector

Table 6 reports the statistical frequency distribution of the radioelement concentration data considering the Compton removal (RC) and RLM approaches, as well as the RLM difference relative to data reported by Cecatto [10]. The range of the 11 classes of the radioelement concentration, considering the RC approach, is from 0 to 22.28%

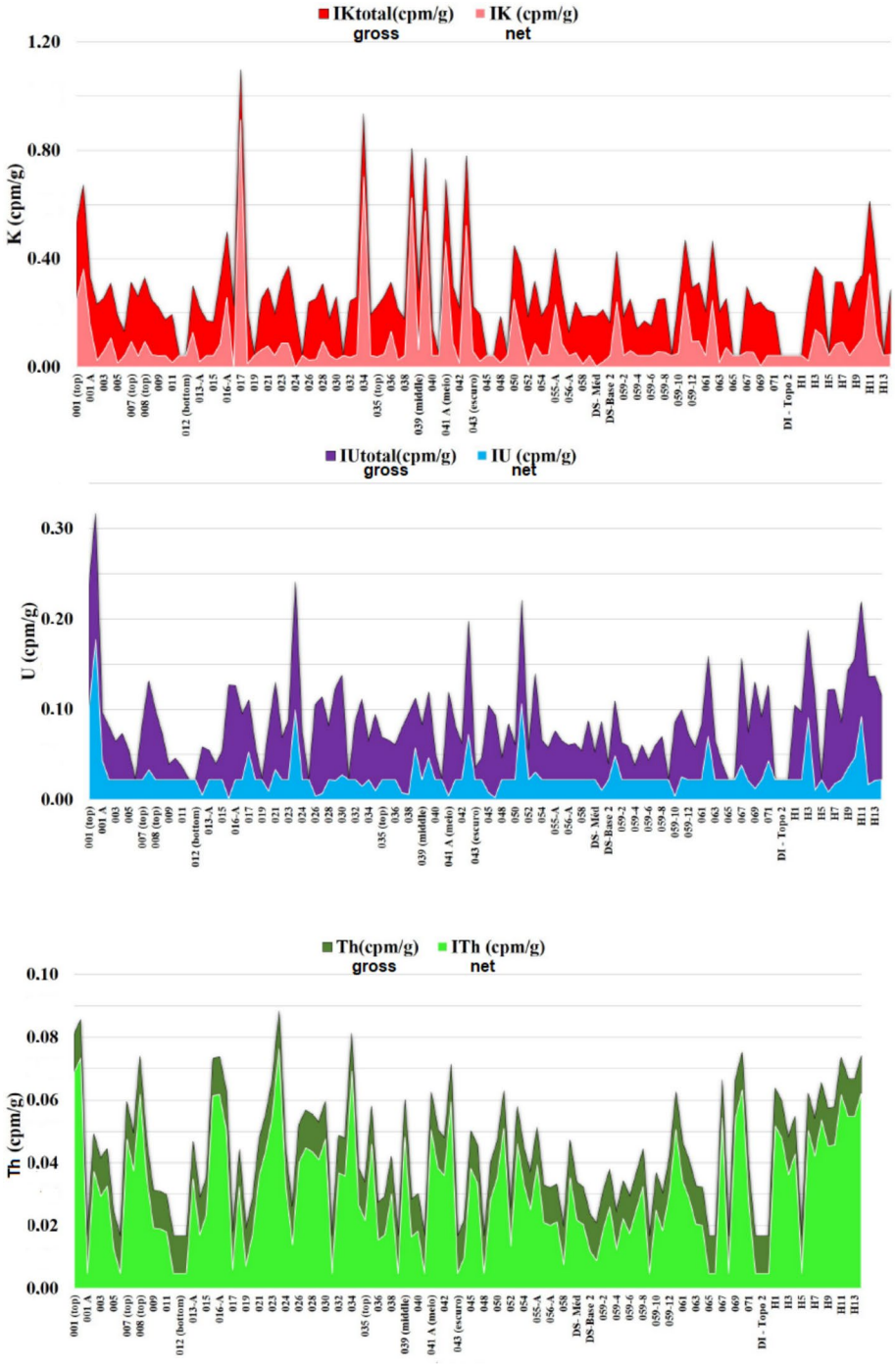

Fig. 4 Comparison of the gross counting rate/weight with the net counting rate/weight in each rock sample from Irati Formation for (*top*) ^{40}K (K), (*middle*) ^{214}Bi (eU), and (*bottom*) ^{208}Tl (eTh)

for K, 0.20 to 102.03 ppm for eU, and 2.42 to 824.86 ppm for eTh (Table 6). When considering the RLM approach, it is 0–21.66% for K, 4.29–131.74 ppm for eU, and 12.01–388.46 ppm for eTh (Table 6), while the 11 classes range for the RLM difference from values given by Cecatto [10] corresponds to 0.01–1.67% for K, 1.11–200.57 ppm for eU, and 1.18–277.69 ppm for eTh (Table 6).

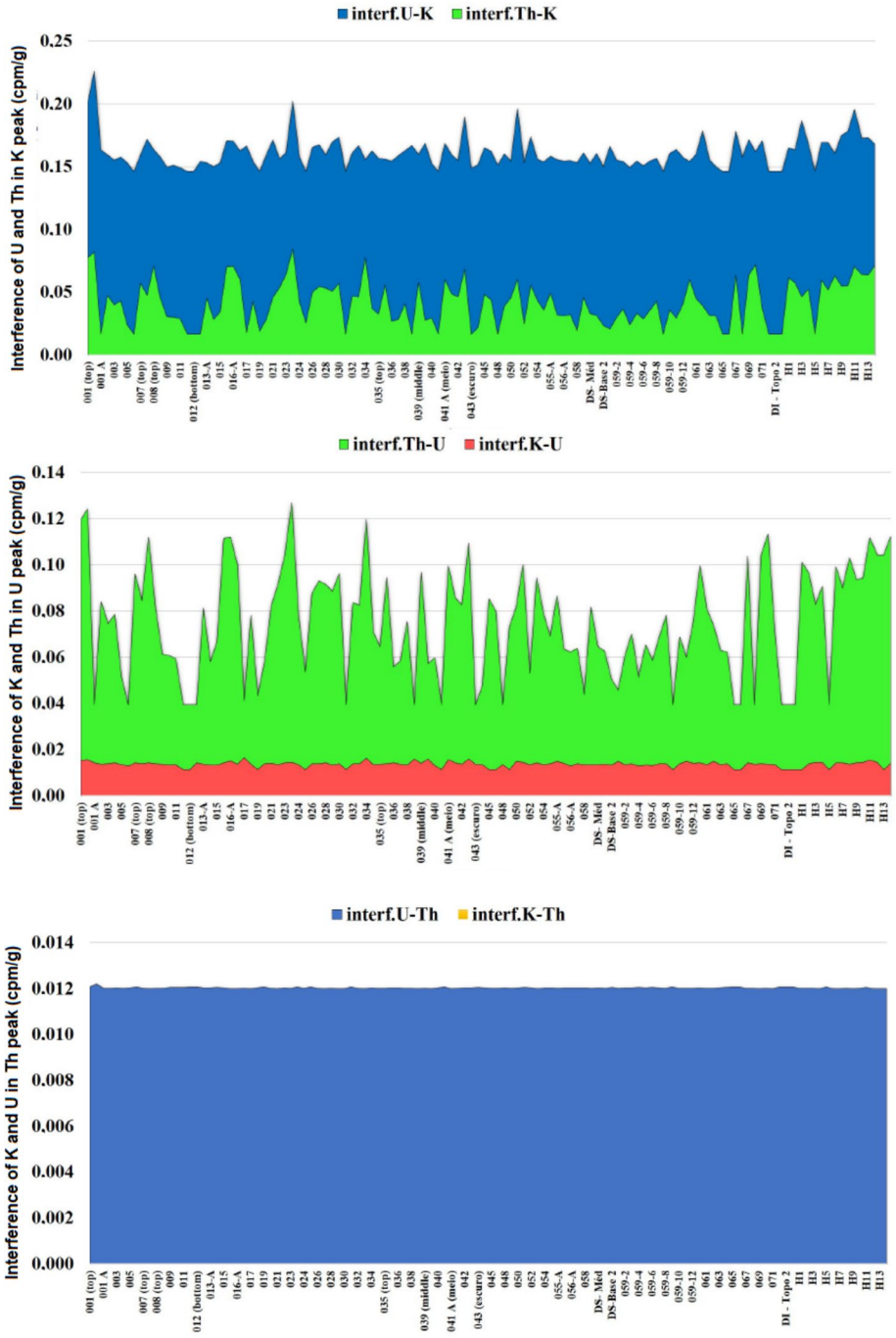

Fig. 5 Compton interference in each rock sample from Irati Formation of (*top*) U and Th in K peak, (*middle*) K and Th in U peak, and (*bottom*) K and U in Th peak

Box plots of the radioelement concentration data obtained by these three approaches are shown in Fig. 6, while Figs. S13-S15 in the Supplementary Material show the K, eU, and eTh data distribution along the distinct sections (upper, middle, and lower) of the wall sampled. Figure 7 illustrates violin plots for clearer visual contrast, integrating all three methods per radioelement. The plots suggest that the data are normally distributed with one mode value and different shapes [5]. For K, the highest difference was found for values obtained by Cecatto [10] compared to those utilizing the methods RC and RLM

Table 6 Frequency distribution of the radioelements concentration according to (top) Compton scattering removal (RC) and (middle) multiple linear regression (RLM) approaches

K (%)					eU (ppm)					eTh (ppm)				
Class	**MEAN**	f_i	F_{AC}	F_i (%)	**Class**	**MEAN**	f_i	F_{AC}	F_i (%)	**Class**	**MEAN**	f_i	F_{AC}	F_i (%)
0.00 |– 2.03	1.01	77	77	64	0.20 |– 9.46	4.83	95	95	79	2.42 |– 77.18	39.8	46	46	38
2.03 |– 4.05	3.04	24	101	84	9.46 |– 18.71	14.08	9	104	87	77.18 |– 151.95	114.57	24	70	58
4.05 |– 6.08	5.06	7	108	90	18.71 |– 27.97	23.34	5	109	91	151.95 |– 226.72	189.34	26	96	80
6.08 |– 8.10	7.09	0	108	90	27.97 |– 37.23	32.6	2	111	93	226.72 |– 301.49	264.1	16	112	93
8.10 |– 10.13	9.12	5	113	94	37.23 |– 46.48	41.86	0	111	93	301.49 |– 376.25	338.87	3	115	96
10.13 |– 12.15	11.14	1	114	95	46.48 |– 55.74	51.11	4	115	96	376.25 |– 451.02	413.64	0	115	96
12.15 |– 14.18	13.17	2	116	97	55.74 |– 65.00	60.37	4	119	99	451.02 |– 525.79	488.4	2	117	98
14.18 |– 16.20	15.19	0	116	97	65.00 |– 74.26	69.63	0	119	99	525.79 |– 600.55	563.17	0	117	98
16.20 |– 18.23	17.22	1	117	98	74.26 |– 83.51	78.89	0	119	99	600.55 |– 675.32	637.94	2	119	99
18.23 |– 20.26	19.24	1	118	98	83.51 |– 92.77	88.14	0	119	99	675.32 |– 750.09	712.7	0	119	99
20.26 |– 22.28	21.27	2	120	100	92.77 |– 102.03	97.4	1	120	100	750.09 |– 824.86	787.47	1	120	100
MAX	22.28					102.03					824.86			
MIN	0					0.20					2.42			
MEAN	2.98					9.64					148.31			
K (%)					**eU (ppm)**					**eTh (ppm)**				
Class	**MEAN**	f_i	F_{AC}	F_i (%)	**Class**	**MEAN**	f_i	F_{AC}	F_i (%)	**Class**	**MEAN**	f_i	F_{AC}	F_i (%)
0.00 |– 1.97	0.98	27	27	23	4.29 |– 15.88	10.09	33	33	28	12.01 |– 46.23	29.12	49	49	41
1.97 |– 3.94	2.95	42	69	58	15.88 |– 27.46	21.67	38	71	59	46.23 |– 80.45	63.34	33	82	68
3.94 |– 5.91	4.92	24	93	78	27.46 |– 39.05	33.26	15	86	72	80.45 |– 114.68	97.56	24	106	88
5.91 |– 7.87	6.89	12	105	88	39.05 |– 50.64	44.84	16	102	85	114.68 |– 148.90	131.79	9	115	96
7.87 |– 9.84	8.86	2	107	89	50.64 |– 62.22	56.43	5	107	89	148.90 |– 183.12	166.01	0	115	96
9.84 |– 11.81	10.83	4	111	93	62.22 |– 73.81	68.02	1	108	90	183.12 |– 217.35	200.24	2	117	98
11.81 |– 13.78	12.80	1	112	93	73.81 |– 85.39	79.60	5	113	94	217.35 |– 251.57	234.46	0	117	98
13.78 |– 15.75	14.77	3	115	96	85.39 |– 96.98	91.19	3	116	97	251.57 |– 285.79	268.68	1	118	98
15.75 |– 17.72	16.73	2	117	98	96.98 |– 108.57	102.77	2	118	98	285.79 |– 320.02	302.91	1	119	99
17.72 |– 19.69	18.70	1	118	98	108.57 |– 120.15	114.36	1	119	99	320.02 |– 354.24	337.13	0	119	99
19.69 |– 21.66	20.67	1	119	99	120.15 |– 131.74	125.95	1	120	100	354.24 |– 388.46	371.35	0	119	99

Table 6 (continued)

K (%)					eU (ppm)					eTh (ppm)				
Class	**MEAN**	f_i	F_{AC}	F_i (%)	**Class**	**MEAN**	f_i	F_{AC}	F_i (%)	**Class**	**MEAN**	f_i	F_{AC}	F_i (%)
MAX	21.66					131.74					388.46			
MIN	0					4.29					12.01			
MEAN	4.62					31.53					67.88			
K (%)					**eU (ppm)**					**eTh (ppm)**				
Class	**MEAN**	f_i	F_{AC}	F_i (%)	**Class**	**MEAN**	f_i	F_{AC}	F_i (%)	**Class**	**MEAN**	f_i	F_{AC}	F_i (%)
	$K_{RLM} - K_{Ceccato}$					$eU_{RLM} - eU_{Ceccato}$					$eTh_{RLM} - eTh_{Ceccato}$			
0.01 |– 0.16	0.09	33	33	28	1.11 |– 19.24	10.18	38	38	32	1.18 |– 26.32	13.75	12	12	10
0.16 |– 0.31	0.24	13	46	38	19.24 |– 37.38	28.31	28	66	55	26.32 |– 51.45	38.89	28	40	33
0.31 |– 0.46	0.39	23	69	58	37.38 |– 55.51	46.44	21	87	73	51.45 |– 76.59	64.02	36	76	63
0.46 |– 0.61	0.54	28	97	81	55.51 |– 73.64	64.57	11	98	82	76.59 |– 101.73	89.16	23	99	83
0.61 |– 0.76	0.69	5	102	85	73.64 |– 91.77	82.71	2	100	83	101.73 |– 126.87	114.3	8	107	89
0.76 |– 0.92	0.84	10	112	93	91.77 |– 109.91	100.84	3	103	86	126.87 |– 152.00	139.44	2	109	91
0.92 |– 1.07	0.99	6	118	98	109.91 |– 128.04	118.97	1	104	87	152.00 |– 177.14	164.57	2	111	93
1.07 |– 1.22	1.14	0	118	98	128.04 |– 146.17	137.11	0	104	87	177.14 |– 202.28	189.71	3	114	95
1.22 |– 1.37	1.29	0	118	98	146.17 |– 164.30	155.24	0	104	87	202.28 |– 227.42	214.85	2	116	97
1.37 |– 1.52	1.44	0	118	98	164.30 |– 182.44	173.37	0	104	87	227.42 |– 252.55	239.98	0	116	97
1.52 |– 1.67	1.59	1	119	99	182.44 |– 200.57	191.50	0	104	87	252.55 |– 277.69	265.12	2	118	98
MAX	1.67					200.57					277.69			
MIN	0.01					1.11					1.18			
MEAN	0.40					33.87					73.41			

In the (bottom) is reported the RLM difference relative to data obtained by Cecatto [10]

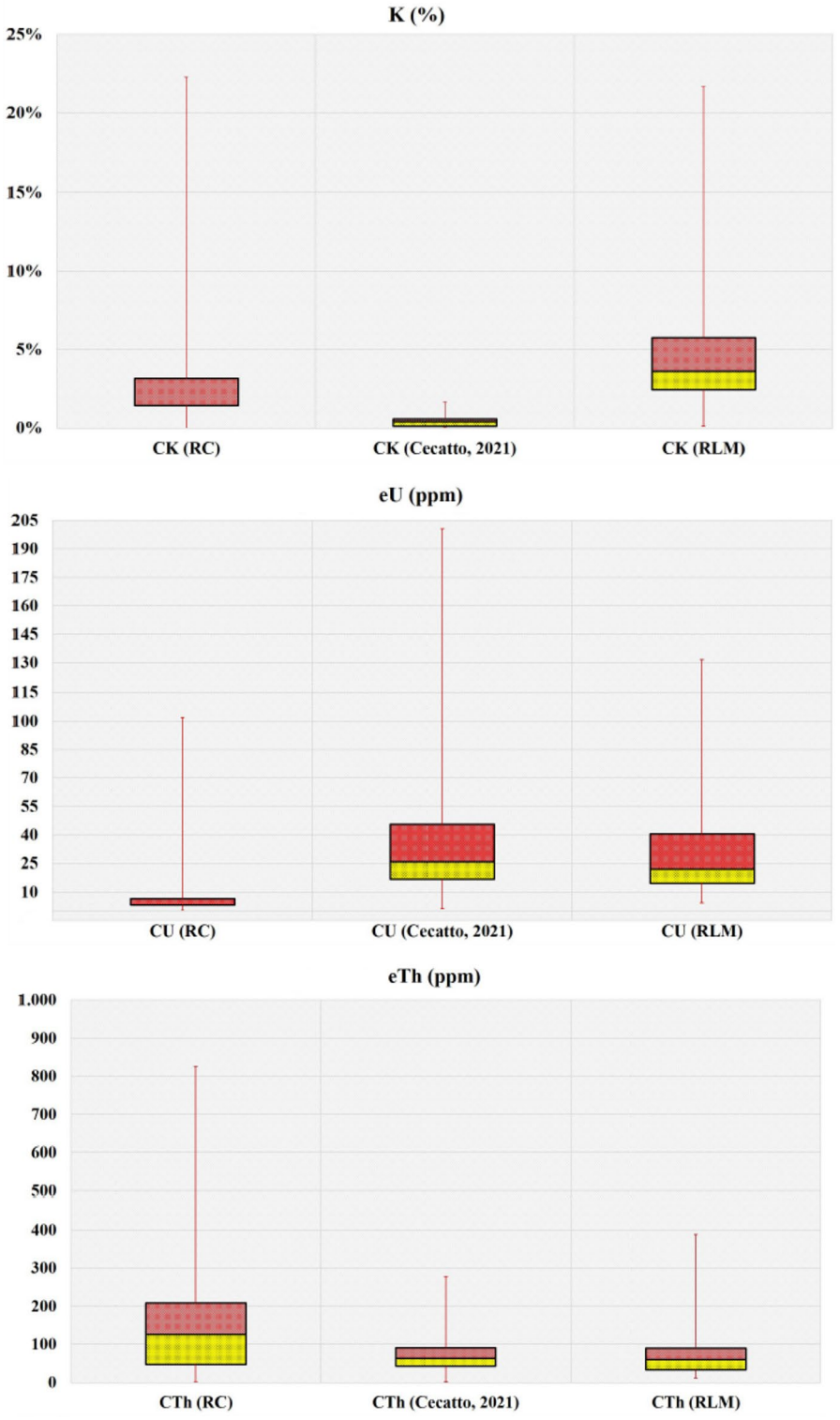

Fig. 6 Box-plots of the quartile distribution and their respective intervals of K, eU, and eTh concentration values as obtained by Cecatto [10] and methods of Compton scattering removal (RC) and multiple linear regression (RLM)

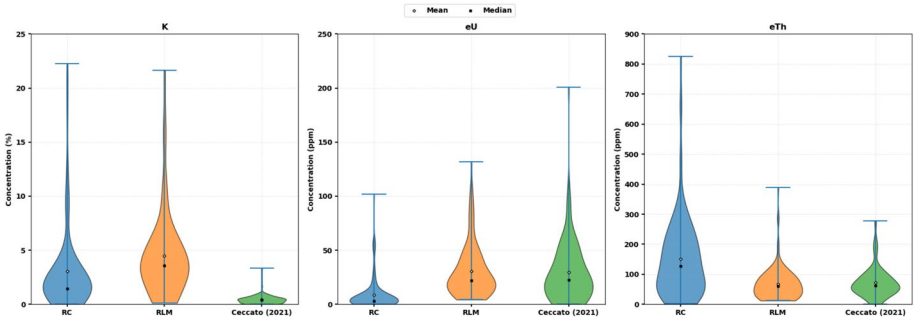

Fig. 7 Violin plots for comparison of the K, eU, and eTh concentration values obtained by Cecatto [10] and the methods of Compton scattering removal (RC) and multiple linear regression (RLM)

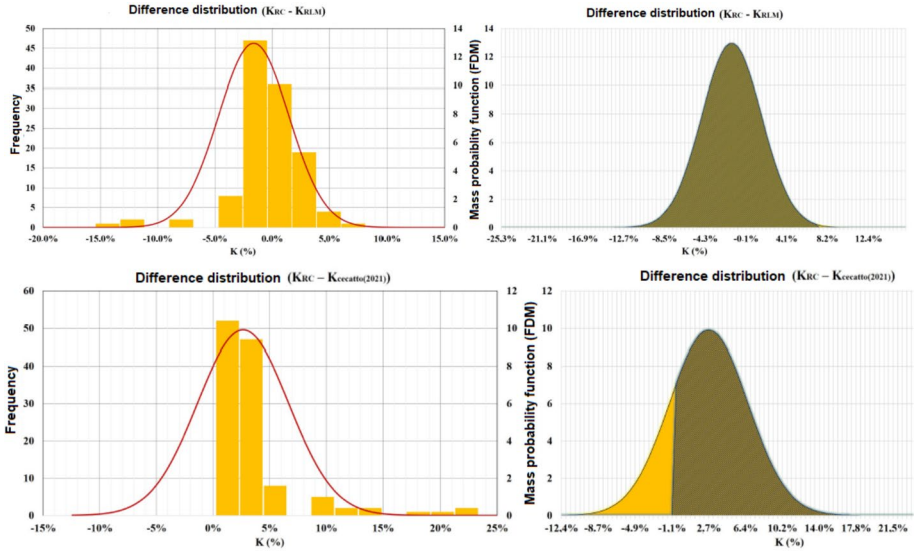

Fig. 8 Gaussian distribution and frequency histogram by class for the subtraction data, sample by sample, considering the data obtained by Cecatto [10] and their treatment by the methods of Compton scattering removal (RC) and multiple linear regression (RLM) of the K concentration values along the wall sampled at Irati Formation, Assistência District

(Fig. 7). For eU and eTh data, the highest difference was verified for data obtained by the method RC relative to RLM and Ceccato [10] (Fig. 7).

Figures 8, 9 and 10 present the Gaussian distribution and frequency of residue values for the 11 different sample classes (Table 6) in the form of histograms. These graphs show the behavior of the results obtained by subtraction between the different approaches utilized [10], and methods RC/RLM). The calibration curves (straight lines) for K, U, and Th, as obtained by Cecatto [10] from the standard concentrations, did not account for the removal of Compton effects in the gamma spectra. On the other hand, such was done when utilizing the RC and RLM methods, which could justify why sometimes they align more closely, reinforcing the usefulness of the correction approach for the analysis of the rock samples.

The minimum and maximum residue values found for the subtraction between the 3 different methods are summarized as follows:

(1) Residues of RC-RLM:

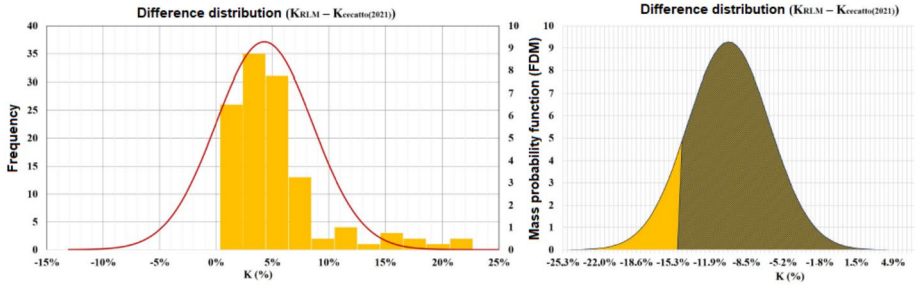

Fig. 8 (continued)

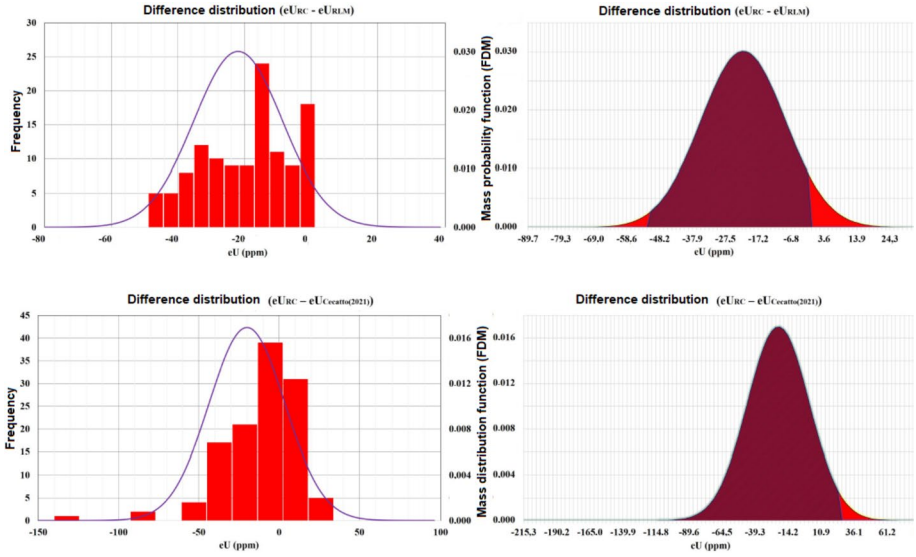

Fig. 9 Gaussian distribution and frequency histogram by class for the subtraction data, sample by sample, considering the data obtained by Cecatto [10] and their treatment by the methods of Compton scattering removal (RC) and multiple linear regression (RLM) of the eU concentration values along the wall sampled at Irati Formation, Assistência District

K(%): Min = −16.51; Max = 6.99
eU(ppm): Min = −51.18; Max = −1.27
eTh(ppm): Min = −16.27; Max = 436.39

(2) Residues of RC-Cecatto [10]:

K(%): Min = −0.84; Max = 22.19
eU(ppm): Min = −148.06; Max = 25.40
eTh(ppm): Min = −154.79; Max = 738.04

(3) Residues of RLM-Cecatto [10]:

K(%): Min = −0.68; Max = 21.57
eU(ppm): Min = −107.89; Max = 69.29
eTh(ppm): Min = −170.81; Max = 301.64

For K, the variation in the residues did not differ significantly between the 3 methods. However, for eU and eTh, the lesser variation in the residues was found between the RC and RLM methods. For K, the residual error reduction was between 1.9% (RC-[10]) and

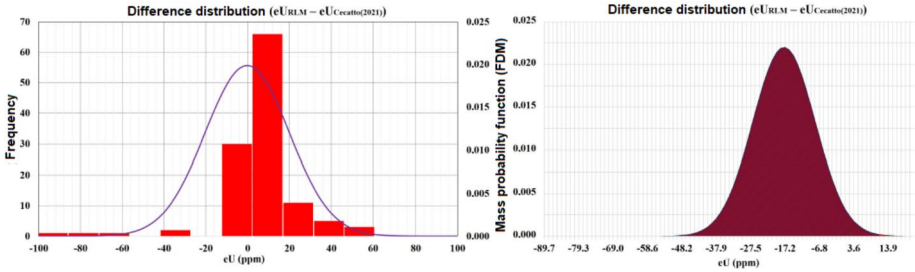

Fig. 9 (continued)

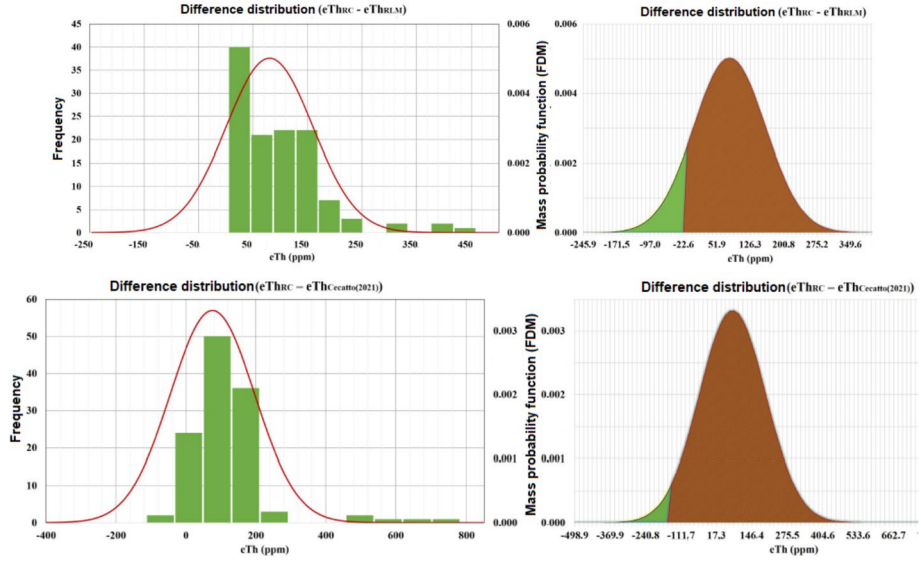

Fig. 10 Gaussian distribution and frequency histogram by class for the subtraction data, sample by sample, considering the data obtained by Cecatto [10] and their treatment by the methods of Compton scattering removal (RC) and multiple linear regression (RLM) of the eTh concentration values along the wall sampled at Irati Formation, Assistência District

3.4% (RLM-[10]), while it was between 4.4% (RLM-[10]) and 97% (RC-[10]) for eTh. The most striking residual error reduction was found for eU, ranging from 248% (RC-[10]) and 255% (RLM-[10]). Such high values could be explained by the difficulty of separating the ^{40}K and ^{214}Bi photopeaks in the gamma-spectra by the traditional methods utilizing the NaI(Tl) detector, as it possesses a low resolution for a clear separation of the gamma-ray energies corresponding to 1461 keV (^{40}K) and 1765 keV (^{214}Bi) [27].

Therefore, possible reasons to explain some abrupt changes in the concentration values for the 3 radionuclides could be:

(1) Frequency of BG measurements: One of the steps that may corroborate such significant differences is the accounting of net counts, or BG-subtracted counts. We noticed that during the gamma analysis period of the samples from Cecatto [10], only 2 measurements were taken over the weeks. This significantly hinders understanding the variations that may occur in the system, especially due to the interference of radiation from surrounding materials (though to a lesser extent due to shielding), and particularly due to fluctuations in cosmic radiation and drift generated in the NaI(Tl) detector spectra.

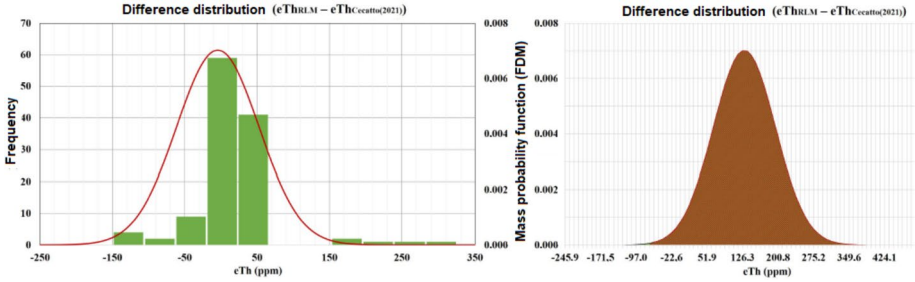

Fig. 10 (continued)

(2) Use of higher amplitude BG on a deficient data set: for the definition of the data incorporated into the methods of this work, and considering the two BG readings taken over weeks, the average was used as a way to reduce the propagation of errors already implicit in any data measurement condition. However, the results of Cecatto [10] were based on the individual use of BG, largely determined using the higher amplitude values (ranging between 1.5 and 2.0 times higher).

(3) Consideration of Compton effect interference and gamma energies that overlap the peaks of interest: this factor is one of the most challenging aspects for data interpretation and correlation with methods that invariably attempt to associate counts independently with the radionuclides of interest, disregarding their other gamma emissions and the Compton continuum generated by them. Removing interfering counts in the windows of interest with subsequent calibration of the system through interpolation of the current standard readings results in more accurate models, but may amplify the distinctions of the absolute values calculated for each sample.

(4) The drift of the gamma spectrometric system, and the need for re-measurements for unsatisfactory integrations or interpolation with significant differential margin: one of the phenomena that interferes with more efficient inte-gration of gamma spectrometric intervals relates to spectral drift, that is a phenomenon depending on the use of appropriate methodsin order to achieve integrations with reduced error propagation and interval discrimination.

(5) Use of additional standards with intermediate concentrations defined for pure or associated radionuclides: System calibration is a fundamental and necessary step for data quantification. However, standards do not always present concentration values consistent with environmental samples collected in the field. Defining standards with intermediate values for the 3 natural radionuclides is crucial to interpolate the data with satisfactory correlation and generate accurate mathematical models for later application to sample data.

(6) Uniformity of geometry, weight, and container materials for hermetically sealing samples: an appropriate and differentiating requirement for better gamma reading is the uniformity of the parameters in which samples are stored. Different weights, with a higher presence of non-emitting inert materials, can contribute to variations in the gamma energies reaching the scintillation crystal. The type of material constituting the vessels can also exert some contribution, as the cans storing the uranium and thorium standards were different when compared to those of the potassium standards and samples. The density of the ma- terial, related to the atomic nuclei present, contributes not only to the shielding of gamma radiation emitted by the radionuclides

of interest but may also increase the incidence of energies from Compton interactions that can cause events in other reading intervals, as well as reduce the counts of the associated radionuclide.

Therefore, it is also important to consider these aspects in the gamma spectrometric analyses in order to meet the ongoing need of improving the methodology for further research, as well as to generate reliable and confident data for the production of technological and scientific knowledge.

The three counting windows (or ROI) for the analysis of the gamma-ray spectra focused on this investigation have also been commonly utilized in other studies reported in the literature, for instance, by Rybach [47, 48] and Chiozzi et al. [12], among others, reinforcing the relevance of the approach described here. The application of the algorithm and models was only defined for the windows analysis; thus, the full spectrum analysis is a challenge for future searches. For U readings using a NaI(Tl) detector, Bezuidenhout [9] described the adoption of the 352 keV gamma-ray peak of ^{214}Pb instead of the 1765 keV ^{214}Bi photopeak, finding that the activity concentrations extracted from ^{214}Pb demonstrated a tendency to be on average 5% lower than the activity concentrations that were extracted from ^{214}Bi. This is another interesting ROI window for future tests of the approach described in this paper, as well as a comparison with results obtained utilizing high-resolution gamma-ray spectrometry by an HPGe detector as reported by Chiozzi et al. [12].

Another highlight of the approach developed here is that it adopts non-sophisticated methodological steps, such as the use of the division of the Compton background into several different segments, after subtraction of the photopeak, and normalization to a fixed number of emitted photons, with later adjustment of the gain of each segment separately to match up the position of common features like the backscatter peak and Compton edge [24]. Additionally, it does not require the use of additional instrumentation for gamma-ray readings, such as scintillator materials surrounding the detector and/or electronic units for anti-coincidence measurements [20, 43].

This investigation reported two approaches utilized for Compton scattering removal from gamma spectra obtained under controlled laboratory conditions for data acquisition, highlighting the importance of improving confidence in the radiometric results. The findings obtained are also relevant in radioactivity readings used in basin-scale geophysical surveys. However, they are commonly realized by airborne spectrometric systems, which demand other requirements for data acquisition and treatment. Despite the differences, the importance of Compton removal initiatives for analyzing gamma-ray spectra has been recognized in such cases, for instance, by Coetzee [14], who adapted an existing approach to Compton continuum removal, used in high-resolution laboratory systems, for the lower spectral resolution of NaI(Tl) based systems. Coetzee [14] described a simple numerical procedure to locate peaks and the associated Compton continuum, utilizing a simple model of the shape of the continuum, which is then subtracted from the total spectrum, requiring minimal user interaction.

Additional useful applications of the removal of the Compton effects in gamma-ray spectra include investigations related to remote sensing, environmental monitoring, and nuclear sites assessment. For example, Bender et al. [8] report that in measured gamma-ray spectra from spent nuclear fuel, the Compton continuum from dominant fission product photopeaks obscures the lower energy lines from other isotopes. These

authors described experiments for the application of Compton suppression to gamma-ray measurements of spent fuel to reduce this effect and allow other, less intense, lower-energy gamma-ray peaks to be detected, potentially improving the accuracy of analysis algorithms.

5 Conclusion

Gamma ray measurements of the natural radioelements potassium (^{40}K), uranium (eU, ^{214}Bi), and thorium (eTh, ^{208}Tl) are a fundamental task in Nuclear Geophysics, consisting on an important tool utilized for geological mapping and mineral resources prospection. However, precise analysis through gamma spectrometry is challenging due to several factors such as the such as energy resolution, linearity, detection efficiency, response time, total number of counts within spectral windows, and chiefly, the continuum Compton in gamma spectra. This paper highlighted procedures developed for minimizing the influence of the Compton effect in the generation of gamma spectrometric data. Methods for selecting regions of interest (ROIs) and the application of automation algorithms to generate mathematical models for gamma spectrum analysis were presented to improve the measurement accuracy, focusing on the use of a portable gamma spectrometer with a NaI(Tl) scintillator, which is a type of detector widely used for characterizing the radioactivity due to those radioelements. The methodology aimed to optimize the precision of analyses from readings taken from a set of standards that allowed to definition of equations able to realize the Compton removal (RC) in the gamma spectra, as well as to apply the multiple regression analysis (RLM) approach in order to calibrate the gamma ray spectrometer. Thus, the experimental steps yielded reliable equations to calculate the radioelement concentration from counting rates obtained for ^{40}K, ^{214}Bi (eU) and ^{208}Tl (eTh). Afterwards, 111 rock specimens collected along one wall in three distinct sections from Irati Formation, Assistência District, Rio Claro city, São Paulo State, Brazil, allowed to apply the equations obtained to remove the interference of the continuum Compton in the photopeaks identified. The samples corresponded to different rock types such as limestone, shale and diabase, a large number of gamma spectra readings of rock samples from Irati Formation, Assistência District, Rio Claro city, São Paulo State, Brazil, allowed to apply the equations obtained in order to remove the interference of the continuum Compton in the photopeaks identified. Nowadays, this geological formation has been extensively investigated by geoscientists for understanding the oil occurrence in limestone fractures, aiming to transfer the knowledge to identify processes taking place in the deep ocean that constitute challenges for the Pre-Salt programs developed by oil companies worldwide. As a consequence of the refining techniques implemented, for the eU and eTh data, it was found lesser variation in the residues calculated by statistical analysis according to the RC and RLM methods, when compared with the data treatment realized without this approach. Thus, this methodology not only contributes to Geophysics but also to other geological and environmental understanding, with significant implications for radiological safety because of the reliable techniques to obtain meaningful results.

Supplementary Information

The online version contains supplementary material available at https://doi.org/10.1007/s44288-025-00249-9.

Supplementary file1 (PDF 2206 KB)

Acknowledgements
CAPES (Coordination for the Development of Graduate People), Brasília (DF), Brazil, is thanked by the PhD Scholarship to EQB.

Author contributions
G.R.C. acquired the gamma spectrometric data E.Q.B. made the data treatment and prepared all tables and figures D.M.B. wrote the main manuscript.

Funding
No funder has provided any grant to develop this research.

Data availability
Data is provided within the manuscript and supplementary information files.

Code availability
Not applicable.

Declarations

Ethics approval and consent to participate
This is an observational study that did not involve human participants or biological materials, thus, not requiring ethical approval of the Research Ethics Committee of the authors' institution.

Consent for publication
Not applicable.

Competing interests
The authors declare no competing interests.

Received: 13 April 2025 / Accepted: 15 September 2025
Published online: 26 September 2025

References

1. Acton QA. Radioactive elements: advances in research and applications. Atlanta: Scholarly Editions; 2013.
2. Adams JAS, Freyer GE. Portable ray spectrometer for field determination of thorium, uranium and potassium. In: Adams JAS, Lowder WM, editors. The natural radiation environment. Chicago: University of Chicago Press; 1964. p. 577–96.
3. Adams JAS, Gasparani P. Gamma rays spectrometry of rocks. Amsterdam: Elsevier; 1970.
4. Aldhuhaibat MJR, Amana MS, Farhan AJ, Jubier NJ. Study of cross section areas ratios for scattering interactions of gamma photons in He, Fe, Fm, H_2O materials. IOP Conf Ser Mater Sci Eng. 2020;757:e012013.
5. AMGEN (AMGEN Scholars Program). How to interpret violin charts. 2025. https://www.labxchange.org/library/items/lb:LabXchange:46f64d7a:html:1. Accessed 9 July 2025.
6. Barbosa O, Gomes FA. Petroleum research at Corumbataí River basin. DNPM/DGM Bulletin. 1958;171:1–40 (**in Portuguese**).
7. Barbosa EQ, Bonotto DM, Roveratti G. Standardization of a NaI(Tl) scintillation detector and its use on environments for geology teaching in a Brazilian university. Environ Earth Sci. 2018;77:e113.
8. Bender S, Heidrich B, Unlu K. Compton suppressed LaBr 3 detection system for use in nondestructive spent fuel assay. Nucl Instrum Methods Phys Res A. 2015;784:474–81.
9. Bezuidenhout J. Measuring naturally occurring uranium in soil and minerals by analyzing the 352 keV gamma-ray peak of ^{214}Pb using a NaI(Tl)-detector. Appl Radiat Isot. 2013;80:1–6.
10. Cecatto GR. Comparative analysis of different gamma-spectrometers on the study of Irati Formation, Paraná basin. MSc Dissertation. Rio Claro: UNESP-São Paulo State University; 2021. https://pubmed.ncbi.nlm.nih.gov/35970115/. Accessed 3 July 2025. (**in Portuguese**)
11. Cherdyntsev VV. Uranium-234. Jerusalem: IPST-Israel Program for Scientific Translations; 1969.
12. Chiozzi P, De Felice P, Fazio A, Pasquale V, Verdoya M. Laboratory application of NaI(Tl) γ-ray spectrometry to studies of natural radioactivity in geophysics. Appl Radiat Isot. 2000;53:127–32.
13. Chu SYF, Ekström LP, Firestone RB. The Lund/LBNL Nuclear Data Search. 1999. http://nucleardata.nuclear.lu.se/nucleardata/toi/index.asp. Accessed 18 July 2022.
14. Coetzee H. Empirical correction for Compton effects in airborne radiometric data. In: Proceedings of the 11th SAGA Biennial Technical Meeting and Exhibition. Swaziland. 2009. p. 444–449.
15. Currie LA. Limits for qualitative detection and quantitative determination. Anal Chem. 1968;40:586–93.
16. Cocco G, Fanfani L, Zanazzi PE. Potassium. In: Wedepohl KH, editor. Handbook of geochemistry, vol 2 (ch 9). New York: Springer-Verlag; 1969.
17. Darnley AG. Uranium exploration data, international geochemical mapping and the environment. In: IAEA, editor. Application of uranium exploration data and techniques in environmental studies. IAEA-TECDOC-827. Vienna: IAEA; 1993.
18. Dentith M, Mudge ST. Geophysics for the mineral exploration geoscientist. Cambridge: Cambridge University Press; 2014.
19. Duval JS, Carson JM, Holman PB, Darnley AG. Terrestrial radioactivity and gamma-ray exposure in the United States and Canada. 2005. U.S. Geological Survey Open-File Report, 1413.
20. Firestone RB. Physics of gamma-ray spectroscopy. 2025. https://indico.ictp.it/event/a04183/session/35/contribution/20/material/0/0.pdf. Accessed 3 July 2025.
21. Gabelman JW. Migration of uranium and thorium: exploration significance. Studies in Geology No. 3. Tulsa (OK): AAPG (American Association of Petroleum Geologists); 1977.

22. Grasty RL, Darnley AG. Calibration of gamma-ray spectrometers for ground and airborne use. Geol Surv Can Pap. 1971;71–17:1–27.
23. Hannasch A, Laso Garcia A, LaBerge M, Zgadzaj R, Köhler A, Couperus Cabadag JP, et al. Compact spectroscopy of keV to MeV X-rays from a laser wakefield accelerator. Sci Rep. 2021;11(1):1–17.
24. Heath RL, Helmer RG, Schmittroth LA, Cazier GA. A method for generating single gamma-ray shapes for the analysis of spectra. Nucl Instrum Methods. 1967;47:281–304.
25. Heier KS, Billings GK. Potassium. In: Wedepohl KH, editor. Handbook of geochemistry, vol 2 (ch 9). New York: Springer-Verlag; 1969.
26. Holz M, França AB, Souza PAde, Iannuzzi R. A stratigraphic chart of the late carboniferous/permian succession of the eastern border of the Paraná basin, Brazil, South America. J South Am Earth Sci. 2010;29:381–99.
27. IAEA (International Atomic Energy Agency). Construction and use of calibration facilities for radiometric field equipment. Technical Report Series No. 309. Vienna: IAEA; 1989.
28. IAEA (International Atomic Energy Agency). Guidelines for radioelement mapping using gamma ray spectrometry data. IAEA-TECDOC-1363. Vienna: IAEA; 2003.
29. Ivanovich M, Harmon RS. Uranium series disequilibrium: applications to environmental problems. 2nd ed. Oxford: Clarendon Press; 1992.
30. Karpius PJ, Reilly TD. Gamma-ray interactions with matter. In: Geist WH, Santi PA, Swinhoe MT, editors. Nondestructive assay of nuclear materials for safeguards and security. Cham: Springer; 2024.
31. Killeen PG. Gamma ray spectrometric methods in uranium exploration-application and interpretation. In: Hood PJ, editor. Geophysics and geochemistry in the search for metallic ores. Economic Geology Report 31, Geological Survey of Canada; 1979. p. 163–229.
32. Killeen PG, Carmichael CM. Gamma-ray spectrometer calibration for field analysis of thorium, uranium and potassium. Can J Earth Sci. 1970;7(4):1031–184.
33. Knoll GF. Radiation detection and measurement. 5th ed. New York (NY): Wiley; 2020.
34. Kogan RM, Nazarov IM, Fridman SD. Gamma spectrometry of natural environments and formations. Jerusalem: IPST-Israel Programme for Scientific Translations; 1971.
35. Ku TL. The uranium – series methods of age determination. Annu Rev Earth Planet Sci. 1976;4:347–79.
36. Lages LC. Irati Formation (Passa Dois Group, Permian, Paraná Basin) at FP-01-PR drill hole (Sapopema, PR). MSc Dissertation. Rio Claro: UNESP-São Paulo State University. 2004. https://repositorio.unesp.br/entities/publication/d4f89d81-1a89-4e4e-badc-2cbca69f363e/full. Accessed 3 July 2025 (**in Portuguese**).
37. L'Annunziata MF. Handbook of radioactivity analysis. 3rd ed. Amsterdam: Elsevier; 2012.
38. Leo WR. Techniques for nuclear and particle physics experiments. 2nd ed. Heidelberg: Springer; 1994.
39. Milani EJ, Melo JHG, Souza PA, Fernandes LA, França AB. Paraná basin. Petrobras Geosci Bull. 2007;15(2):265–87 (**in Portuguese**).
40. Omran AA, Farag SS. Geology, radioactive mineralogy and geochemistry of the granitic rocks of Gabal, Khashm El-risha area, north eastern desert, Egypt. Delta J Sci. 2007;31:30–56.
41. ORTEC (Oak Ridge Tennessee Company). Experiments in nuclear science – a laboratory manual. Oak Ridge: EG&G ORTEC; 1984.
42. Perez-Andujar A, Pibida L. Performance of CdTe, HPGe and NaI(Tl) detectors for radioactivity measurements. Appl Radiat Isot. 2004;60:41–7.
43. Radford DC, Ahmad I, Holzmann R, Janssens RVF, Khoo TL. A prescription for the removal of Compton-scattered gamma rays from gamma-ray spectra. Nucl Instrum Methods Phys Res A. 1987;258:111–8.
44. Rogers JJW, Adams JAS. Thorium. In: Wedepohl KH, editor. Handbook of geochemistry, vol 4 (ch 90). New York: Springer-Verlag; 1969.
45. Rogers JJW, Adams JAS. Uranium. In: Wedepohl KH, editor. Handbook of geochemistry, vol 4 (ch 92). New York: Springer-Verlag; 1969.
46. Roveratti G, Bonotto DM. Comparative analysis of gamma ray spectrometers applied to Irati Formation, Paraná Basin, São Paulo State, Brazil. Appl Radiation Isotopes. 2022;188:e110399.
47. Rybach L. Radiometric techniques. In: Wainerdi RE, Uken EA, editors. Modern methods of geochemical analysis. New York: Plenum Press; 1971.
48. Rybach L. Determination of the heat production rate. In: Haenel R, Rybach L, Stegena L, editors. Handbook of terrestrial heat-flow density determination. Dordrecht: Kluwer Academic Publishers; 1988.
49. Souza IVAF, Mendonça Filho JG, Menezes TR. Evaluation of the thermal effect of igneous intrusives in a potentially generating horizon from the Paraná basin. Braz J Geol. 2008;38(2):138–48.
50. Strobino EDF. Survey of radiometric profiles in Permian sediments from Paraná Basin, east of São Paulo State. Braz J Geophys. 2006;24:144.
51. Sudarshan M, Joseph J, Singh R. Full energy peak efficiency of NaI(Tl) gamma detectors and its analytical and semi-empirical representations. J Phys D. 1992;25:1561–7.
52. Tauhata L, Salati IPA, Di Prinzio R, Di Prinzio A. Radioprotection and dosimetry: fundamentals. 3rd ed. Rio de Janeiro: IRD/CNEN; 2001. (**in Portuguese**).
53. Ward SH. Gamma-ray spectrometry in geologic mapping and uranium exploration. Salt Lake City (UT): University of Utah; 1981.
54. Wilhelm AS, Jovanovic I. Gamma-ray spectroscopy using agular distribution of Compton scattering. Nucl Inst Methods Phys Res A. 2022;1031:e166502.
55. Young DH. Statistical treatment of experimental data. New York: McGraw-Hill; 1962.

Publisher's Note

Springer Nature remains neutral with regard to jurisdictional claims in published maps and institutional affiliations.